Whispering Gallery Modes in Nanosized Dielectric Resonators with Hexagonal Cross Section

Thomas Nobis,* Evgeni M. Kaidashev,† Andreas Rahm, Michael Lorenz, and Marius Grundmann

Fakultät für Physik und Geowissenschaften, Institut für Experimentelle Physik II, Universität Leipzig, Linnéstraße 5, D-04103 Leipzig, Germany

(Received 12 May 2004; published 3 September 2004)

The size dependence of whispering gallery modes in dielectric resonators with hexagonal cross section has been observed within the visible spectral range for cavity diameters comparable to the light wavelength. As a model system single, tapered, high aspect ratio zinc oxide nanoneedles were analyzed. They enable systematic investigations as a function of the resonator diameter down to the nanometer regime. A simple plane wave interference model without free parameter describes the spectral positions and the linewidths of the modes in good agreement with the experiment.

DOI: 10.1103/PhysRevLett.93.103903 PACS numbers: 42.25.Hz, 42.25.Ja, 42.55.Sa

In musical instruments, in microwave generators, and, of course, in various kinds of lasers, resonators and their eigenmodes play an important role as an integral part of various technical applications. In the last few decades, as a result of miniaturization within the field of electronics and photonics, very small optical resonators strongly gained importance. In this context, an interesting type of resonator is the so-called dielectric whispering gallery resonator, e.g., shaped as a microdisk [1–4], microcylinder [5], or microsphere [6,7]. Inside such a resonator, the light wave can be considered to circulate around due to multiple total internal reflection (TIR) at the resonator's boundary. This effect typically leads to high Q factors and low laser threshold power. In recent years, particularly in the course of analyzing and employing wurtzite structured materials, research focused on hexagonally shaped resonators, and whispering gallery mode (WGM) lasing has been successfully demonstrated also in hexagonal cavities [8,9]. However, the size of all aforementioned cavities is typically much larger than the considered light wavelength λ. In order to create nanosized and laterally single mode devices, e.g., a nanolaser as demonstrated in Ref. [10], the prospering branch of nanophotonics requires resonators, whose lateral size is at least comparable to or even smaller than λ. In this regime WGMs have been explored little so far.

In this Letter we present the first systematic investigation of WGMs in hexagonal resonators for small mode numbers N down to $N = 1$. Single, high aspect ratio zinc oxide (ZnO) nanoneedles have been analyzed, whose tapered cross section easily allows studies of resonator properties in dependence of the cavity diameter. In our measurements, the continuous transition from a multimode to a single mode cavity is directly observed. Surprisingly, a simple plane wave interference model without free parameters agrees well with our experimental data for all N.

Figure 1 depicts schematically the hexagonal cavity, i.e., a dielectric hexagon surrounded by air. Theoretical work on this kind of open resonator has been the subject of present-day literature [11]. To calculate the resonant WGMs, Maxwell's equations have to be solved numerically [11,12]. When the refractive index of the considered material exhibits a spectral dependence, as is in the case of ZnO, for every cavity diameter this procedure has to be performed for all wavelengths of interest. However, a simple plane wave model (PWM) has been deduced from theoretical investigations [11]. Its main idea is that a light wave interferes with itself when having completed one full circulation within the resonator. To enforce constructive interference the total phase shift of the wave along its path has to be an integer multiple of 2π; i.e., only entire wave trains are allowed to perform multiple circulations generating a standing wave. Taking into account the polarization-dependent negative phase shift that occurs during the process of TIR [13], we obtain the following equation:

$$6R_i = \frac{hc}{nE}\left[N + \frac{6}{\pi}\arctan(\beta\sqrt{3n^2 - 4})\right]. \qquad (1)$$

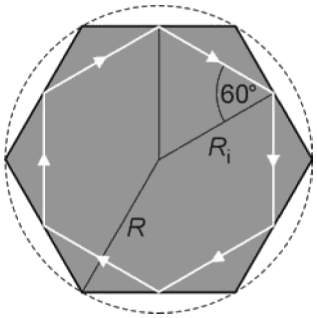

FIG. 1. The light confined within a hexagonal cross section can be assumed to circulate inside the cavity as indicated by the white arrows. The refractive index of ZnO for light in the visible spectral range varies around $n \approx 2$ [20]. Therefore, the smallest critical angle of TIR is about 30°. The angle of incidence of the circulating light is 60° and, hence, the regime of TIR is easily achieved. The geometry of the cavity can be described by the radius of the incircle R_i, by the radius of the circumscribing circle R, or by its related diameter $D = 2R$ using the geometric relation $R_i = \sqrt{3}R/2$. Note that the circumference of the inscribed white hexagon has a length of $6R_i$.

The factor β regards polarization, for TM polarization, i.e., ($\vec{E} \parallel \vec{c}$), $\beta = \beta_{\mathrm{TM}} = n^{-1}$ has to be used; TE polarization ($\vec{E} \perp \vec{c}$) leads to $\beta = \beta_{\mathrm{TE}} = n$. Because of the spectral dependence of the refractive index $n = n(E)$, Eq. (1) is an implicit equation to determine the discrete resonance energies $E = E_N(R_i)$ in terms of the geometric parameter R_i (see Fig. 1), Planck's constant h, and vacuum speed of light c. The first factor of the right side of Eq. (1) corresponds to the wavelength in matter. The integer $N \geq 1$ characterizes the interference order of the resonance, which is in this case identical with the respective WGM number [11]. The following term containing β refers to the additional phase shift mentioned above. Furthermore, since ZnO is uniaxial, $n = n_{\parallel}(E)$ and $n = n_{\perp}(E)$ have to be applied for TM and TE polarization, respectively. We note that Eq. (1) for TM polarization and $n = \mathrm{const}$ is identical with Eq. (17) of Ref. [11]. Neglecting the spectral dependency of n, Eq. (1) leads to

$$E_N \propto \frac{1}{R_i}, \tag{2}$$

and thus WGMs shift to higher energies with decreasing cavity diameter.

Although TIR suggests no way for the light to leave the resonator, emission nevertheless occurs at the corners of the hexagon [11]. Hence, it is possible to optically detect the WGMs. Since the geometrical model leading to Eq. (1) is a combination of basic ray and plane wave optics, it is expected to be applicable only for $R \gg \lambda$, i.e., for $N \gg 1$ [11]. Anyhow, we show in this work that Eq. (1) describes the experimentally found WGMs down to mode number $N = 1$.

Scanning electron microscopy (SEM) images of the investigated ZnO nanoneedle are shown in Fig. 2. The needles have been grown by high pressure pulsed laser deposition (PLD) on a-plane sapphire, utilizing gold assisted growth conditions similar to Ref. [14]. More detailed information about this growth process will be published elsewhere [15]. ZnO is of wurtzite crystal structure, and its preferred growth direction is along the c axis. Hence, the cross section of the given needle is a regular hexagon [Fig. 2(c)]. As can be seen in Figs. 2(b)–2(d), the cross section is continuously tapered when approaching the top of the needle. Since the aspect ratio of the needle is very high, every plane perpendicular to the needle's longitudinal axis creates a hexagonal cavity as decribed above.

ZnO is a direct semiconductor with a band gap of about 3.4 eV and an efficient emitter of ultraviolet light. In bulk material, it commonly shows an additional broad unstructured luminescence band (FWHM $\approx$ 600 meV) within the visible spectral range (VIS) with a spectral maximum around 2.35 eV ($\lambda \cong 530$ nm) due to oxygen or zinc vacancies [16]. In hexagonal ZnO microcrystals with fairly large diameter $D > 1$ μm, WGMs accompany

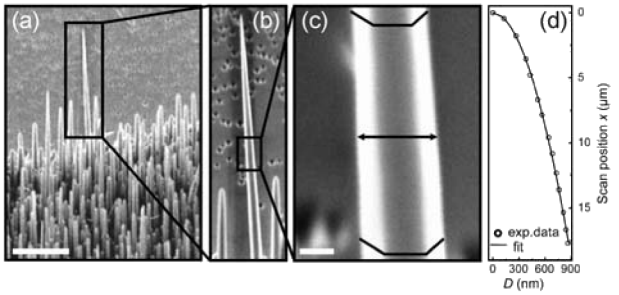

FIG. 2. SEM image of the investigated nanoneedle. All images have been obtained at 45° perspective. (a) SEM image of an array of ZnO nanoneedles containing the reported one marked by a black rectangle. The scale bar has a length of 10 μm. (b) Larger scale SEM image of the investigated nanoneedle. The needle's diameter is continuously tapered approaching zero at the top. (c) High resolution SEM image indicating the hexagonal cross section of the needle. The scale bar has a length of 300 nm. (d) Experimentally determined shape of the needle. The obtained characteristic of the diameter D vs scan position x can be fitted using a potential law $D \propto x^{0.523 \pm 0.007}$, leading to a square-root-like shape of the needle.

this VIS emission as a series of sharp peaks within the broad luminescence band [17]. Nanosized crystals show broadened WGMs due to the increase of losses with decreasing cavity diameter. Nevertheless, we visualized WGMs in the ZnO nanoneedle of Fig. 2 even at diameters $D < \lambda/n \approx 270$ nm. For this purpose, we performed spatially resolved cathodoluminescence (CL) [18,19]; i.e., pointwise CL spectra have been recorded across the whole needle using a scan grid of 16×150 points. Typical spectra and their interpretation are given in Fig. 3. The broad VIS band of luminescence is clearly modulated with varying spectral maxima along the needle's axis. Those maxima appear due to a preferred constructive interference of light whose photon energy fulfills the resonance condition of Eq. (1). For decreasing diameter, approaching the top of the needle, these maxima continuously shift to higher energies. This effect supplies the unambiguous proof that the measured spectral modulation actually originates from WGMs. When the dominating WGM with number N is blueshifted so far that it leaves the VIS range, the next lower resonance $N - 1$ occurs at lower energies indicated by a discontinuous redshift of the spectral maximum in Figs. 3(c) and 3(d). This process continues until $N = 1$ is reached referring to the last resonance that can be observed.

Since theory permits both TM and TE modes, we performed polarization-dependent microphotoluminescence experiments. These show that the WGMs are preferentially TM polarized, as described in Fig. 4. This result is consistent with former investigations of lasing in hexagonal cavities within the micrometer regime, which are reported to emit only TM modes [8]. Hence,

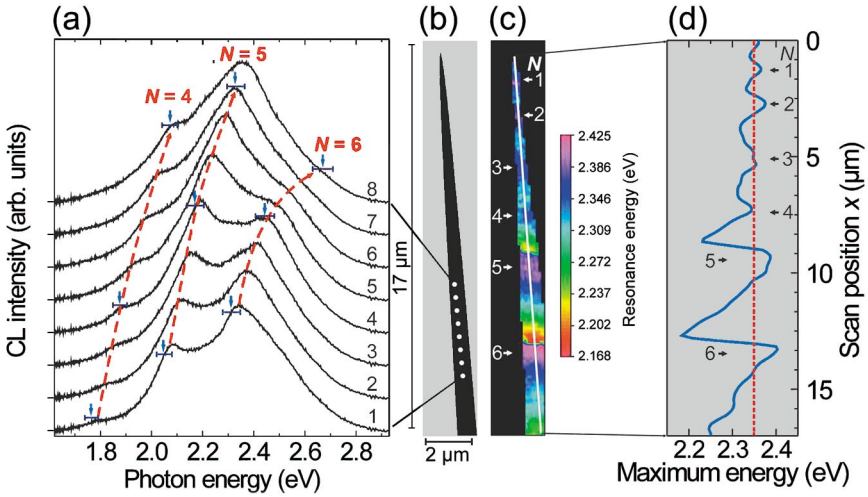

FIG. 3 (color). Spatially resolved cathodoluminescence investigation of a single tapered ZnO nanoneedle. (a) CL spectra shifted vertically for clarity collected at eight equidistant locations marked on the needle's longitudinal axis by white dots in (b). The VIS band of ZnO between 1.8 and 2.9 eV is modulated such that maxima can clearly be distinguished from each other and attributed to WGMs labeled according to Eq. (1). Since the radius of the needle decreases along the longitudinal axis, the spectral maxima continuously shift to higher energies as indicated by the red dashed lines. Blue arrows and error bars mark selected TM-resonance energies obtained from Eq. (1) and their error. (b) Experimentally determined shape of the needle. (c) Map of the energy of the spectral maximum within the visible spectral range. (d) Line scan along the white line shown in (c). The red dashed line gives the maximum position of the unstructured VIS band in bulk material.

in comparison to TE modes, TM modes obviously exhibit lower losses.

To compare the measured energies of the WGMs with the theoretically predicted ones for both types of polarization, a spectral line scan along the needle's longitudinal axis is given in Fig. 5. In gray scale, the resonances

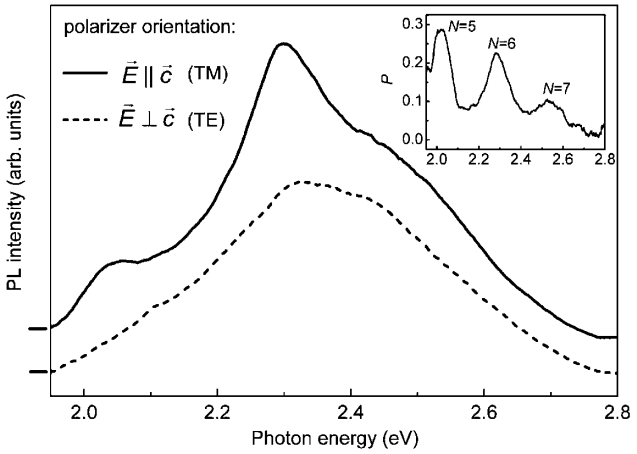

FIG. 4. Microphotoluminescence spectra of the nanoneedle of Fig. 2 for $D \approx 790$ nm at two different polarizer azimuth orientations shifted vertically for clarity. The modulation of the VIS band almost disappears when detecting the TE mode. Thus, the resonances are mainly TM polarized. The inset shows the ratio $P = (I_{TM} - I_{TE})/(I_{TM} + I_{TE})$, which visualizes the TM-WGMs as distinguishable peaks. The polarization effect has been found to be independent of the polarization of excitation.

appear as a set of bright lines that actually exhibit a curvature as expected from Eq. (2). For the calculation of the resonances according to Eq. (1) we use experimentally quantified values of $n_{||}(E)$ and $n_{\perp}(E)$, determined ellipsometrically on c-plane oriented PLD grown ZnO thin film samples [20]. The theoretical values are shown with dots and cross symbols in Fig. 5. The dots (TM) match the measured resonance energies with very good agreement. Additionally, the well fitting blue arrows within Fig. 3(a) confirm that the simple PWM gives a good description of the basic physics of WGMs even in nanosized crystal geometries within the limits of the resonance linewidths.

As mentioned above, there is an energy difference between predicted TM and TE modes. This difference is mostly due to β in Eq. (1), since the ZnO birefringence $(n_{||} - n_{\perp})/(n_{||} + n_{\perp}) \approx 1.2\%$ is small [20]. However, the TE mode with mode number N is predicted to appear very close to the spectral position of the TM mode $N + 1$ (Fig. 5), and hence this could be one reason for the missing TE mode series. Possible TE-WGM maxima should always lie beyond higher ordered TM maxima, and, as the former ones suffer larger losses, they lead to much broader resonance peaks hardly detectable in the VIS band.

For mode numbers $N \geq 4$, single TM-WGMs can be detected unambiguously as distinguishable maxima modulating the broad VIS band. For smaller mode numbers $N \leq 3$, WGMs can be visualized only as a continuous blueshift of the intrinsic VIS maximum, and the discontinuities in Figs. 3(c) and 3(d) become smooth. This is due

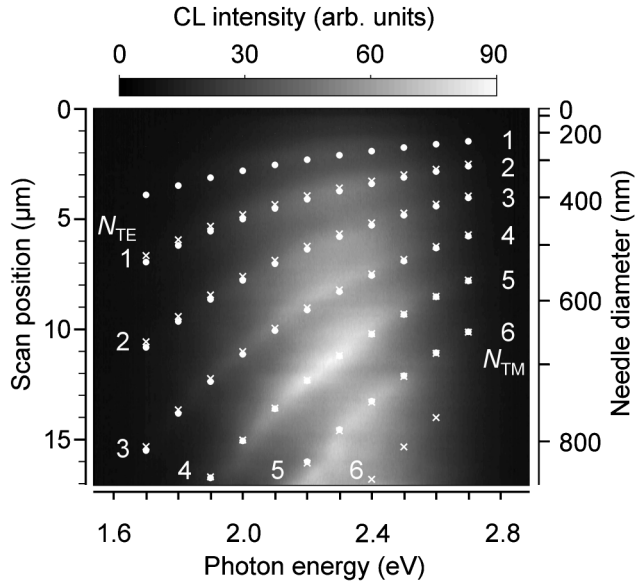

FIG. 5. Two dimensional plot of spectra recorded along a line scan on the needle's longitudinal axis. The left vertical axis shows the line scan position x; the right one refers to the respective needle diameter D. The gray scales refer to the spectral CL intensity. The spectral maxima, i.e., the measured WGM energies, appear as bright belts going from the bottom left corner to the right upper one. With decreasing diameter all resonances shift systematically to higher energies. The white dots give theoretical TM-resonance energy positions obtained from Eq. (1); white crosses give the same for TE polarization. Without adjusting free parameters there is very good agreement between experiment and theory.

to the extreme line broadening of both types of WGMs with decreasing cavity diameter. Theory [11] predicts line broadening by loss processes due to boundary waves that are scattered out of the resonator and due to light paths whose angle of incidence is slightly deviating from 60°. A relation FWHM $\propto E^{-1}R^{-2}$ is obtained, which explains the dramatic broadening of the measured resonances. For TM polarization and $N = 6$ (spectrum 1 of Fig. 3(a)] a FWHM of about 350 meV is predicted. Considering that the underlying theory again is prepared for $N \gg 1$, the obtained spectrum verifies this value within the limits of resolution. For resonance $N = 3$ the theoretical FWHM is about 900 meV, which exceeds even the intrinsic linewidth of the VIS band. This explains the difficulty to obtain distinct WGM peaks for $N \leq 3$. Nevertheless, VIS emission is still affected when a WGM crosses the VIS range, as Fig. 5 clearly shows intensity modulations at the respective line scan positions. We note that losses due to surface roughness of the cavity faces could also lead to line broadening. However, as the high resolution SEM image of Fig. 2(c) shows well shaped resonator faces, we do not adopt this loss process to be the dominating one.

Certainly there are, however, small deviations between the detected peak energies and the predicted TM-WGMs, according to Eq. (1). [See Figs. 3(a) and 5.] These deviations probably reveal the limits of the simple PWM. To discuss this fact more in detail we note that the application of numerical methods to predict resonance energies at the end always depends on a precise determination of the considered geometry, e.g., R_i, and a good knowledge of the refractive index n. SEM measurements of the cavity diameter D are performed with an error of at least 1%. The ellipsometrically determined values for $n_{\|}$ for bulk material yield an error in n of about 2%. The actual refractive index of the nanocrystals may possibly differ additionally. These effects lead to an error in E of about 3%, i.e., 50–80 meV in the considered spectral range, which are indicated as error bars in Fig. 3(a). Compared to the linewidths of the WGMs, Eq. (1) for TM polarization still gives a very good description of the resonant modes.

In conclusion, we could for the first time analyze whispering gallery modes in hexagonal zinc oxide nanoneedles for mode numbers in the range from $N = 1$ to $N = 6$. The energy shift and broadening of the modes for cavity diameter decreasing to zero is well described without free parameter by Eq. (1) from a plane wave model. However, further theoretical modeling seems necessary.

This work was supported by the Deutsche Forschungsgemeinschaft within FOR 522 (Project No. Gr 1011/12-1).

*Corresponding author.
Electronic address: nobis@physik.uni-leipzig.de
†On leave from Rostov-on-Don State University, Mechanics and Applied Mathematics Research Institute, 344090 Rostov-on-Don, Russia.

[1] S. L. McCall *et al.*, Appl. Phys. Lett. **60**, 289 (1992).
[2] S. Chang *et al.*, Appl. Phys. Lett. **75**, 166 (1999).
[3] K. J. Luo *et al.*, Appl. Phys. Lett. **77**, 2304 (2000).
[4] X. Liu *et al.*, Appl. Phys. Lett. **84**, 2488 (2004).
[5] A. F. J. Levi *et al.*, Appl. Phys. Lett. **62**, 2021 (1993).
[6] S. M. Spillane, T. J. Kippenberg, and K. J. Vahala, Nature (London) **415**, 621 (2002).
[7] M. V. Artemyev, U. Woggon, and R. Wannemacher, Appl. Phys. Lett. **78**, 1032 (2001).
[8] I. Braun *et al.*, Appl. Phys. B **70**, 335 (2000).
[9] U. Vietze *et al.*, Phys. Rev. Lett. **81**, 4628 (1998).
[10] M. H. Huang *et al.*, Science **292**, 1897 (2001).
[11] J. Wiersig, Phys. Rev. A **67**, 023807 (2003).
[12] J. Wiersig, J. Opt. A **5**, 53 (2003).
[13] J. D. Jackson, *Classical Electrodynamics* (Wiley, New York, 1999).
[14] P. Yang *et al.*, Adv. Funct. Mater. **12**, 323 (2002).
[15] M. Lorenz *et al.* (unpublished).
[16] B. Lin, Z. Fu, and Y. Jia, Appl. Phys. Lett. **79**, 943 (2001).
[17] Th. Nobis *et al.* (unpublished).
[18] J. Christen *et al.*, J. Vac. Sci. Technol. B **9**, 2358 (1991).
[19] Th. Nobis *et al.*, Nano Lett. **4**, 797 (2004).
[20] R. Schmidt *et al.*, Appl. Phys. Lett. **82**, 2260 (2003).